Atmospheric
Chemistry
and Physics
Discussions

Open Access

Air quality and radiative impacts of Arctic shipping emissions in the summertime in northern Norway: from the local to the regional scale

L. Marelle[1,2], J. L. Thomas[1], J.-C. Raut[1], K. S. Law[1], J.-P. Jalkanen[3], L. Johansson[3], A. Roiger[4], H. Schlager[4], J. Kim[4], A. Reiter[4], and B. Weinzierl[4,5]

[1]Sorbonne Universités, UPMC Univ. Paris 06; Université Versailles St-Quentin; CNRS/INSU, LATMOS-IPSL, Paris, France
[2]TOTAL S.A, Direction Scientifique, Tour Michelet, 92069 Paris La Defense, France
[3]Finnish Meteorological Institute, Helsinki, Finland
[4]Institut für Physik der Atmosphäre, Deutsches Zentrum für Luft- und Raumfahrt (DLR), Oberpfaffenhofen, Germany
[5]Ludwig Maximilians Universität (LMU), Meteorologisches Institut, 80333, München, 14, Germany

Discussion Paper | Discussion Paper | Discussion Paper | Discussion Paper |

ACPD

15, 18407–18457, 2015

Air quality and radiative impacts of Arctic shipping emissions

L. Marelle et al.

Title Page

Abstract | Introduction

Conclusions | References

Tables | Figures

|◄ | ►|

◄ | ►

Back | Close

Full Screen / Esc

Printer-friendly Version

Interactive Discussion

Title Page

Abstract | Introduction

Conclusions | References

Tables | Figures

|◄ | ►|

◄ | ►

Back | Close

Full Screen / Esc

Printer-friendly Version

Interactive Discussion

Abstract

In this study, we quantify the impacts of shipping pollution on air quality and short-wave radiative effect in northern Norway, using WRF-Chem simulations combined with high resolution, real-time STEAM2 shipping emissions. STEAM2 emissions are eval-
5   uated using airborne measurements from the ACCESS campaign, which was conducted in summer 2012, in two ways. First, emissions of NO_x and SO_2 are derived for specific ships from in-situ measurements in ship plumes and FLEXPART-WRF plume dispersion modeling, and these values are compared to STEAM2 emissions for the same ships. Second, regional WRF-Chem runs with and without ship emissions are
10 performed at two different resolutions, $3\,km \times 3\,km$ and $15\,km \times 15\,km$, and evaluated against measurements along flight tracks and average campaign profiles in the marine boundary layer and lower troposphere. These comparisons show that differences between STEAM2 emissions and calculated emissions can be quite large (-57 to $+148\,\%$) for individual ships, but that WRF-Chem simulations using STEAM2 emis-
15 sions reproduce well the average NO_x, SO_2 and O_3 measured during ACCESS flights. The same WRF-Chem simulations show that the magnitude of NO_x and O_3 production from ship emissions at the surface is not very sensitive ($< 5\,\%$) to the horizontal grid resolution (15 or 3 km), while surface PM_{10} enhancements due to ships are moderately sensitive (15 %) to resolution. The 15 km resolution WRF-Chem simulations are used
20 to estimate the local and regional impacts of shipping pollution in northern Norway. Our results indicate that ship emissions are an important local source of pollution, enhancing 15 day averaged surface concentrations of NO_x ($\sim +80\,\%$), O_3 ($\sim +5\,\%$), black carbon ($\sim +40\,\%$) and $PM_{2.5}$ ($\sim +10\,\%$) along the Norwegian coast. Over the same period ship emissions in northern Norway have a shortwave (direct + semi-direct + indirect)
25 radiative effect of $-9.3\,mW\,m^{-2}$ at the global scale.

Title Page

Abstract | Introduction

Conclusions | References

Tables | Figures

◀◀ | ▶▶

◀ | ▶

Back | Close

Full Screen / Esc

Printer-friendly Version

Interactive Discussion

1   Introduction

Shipping is an important source of air pollutants and their precursors, including carbon monoxide (CO), nitrogen oxides (NO_x), sulfur dioxide (SO_2), Volatile Organic Compounds (VOCs); as well as organic carbon (OC) and black carbon (BC) aerosols (Corbett and Fischbeck, 1997; Corbett and Köhler, 2003). It is well known that shipping emissions have an important influence on air quality in coastal regions, often enhancing ozone (O_3) and increasing aerosol concentrations (e.g. Endresen et al., 2003). Corbett et al. (2007) and Winebrake et al. (2009) showed that aerosol pollution from ships might be linked to cardiopulmonary and lung diseases globally. Because of their negative impacts, shipping emissions are increasingly subject to environmental regulations. The International Maritime Organization (IMO) has designated several regions as Sulfur Emission Control Areas (SECAs, including the North Sea and Baltic Sea in Europe), where low sulfur fuels must be utilized to minimize the air quality impacts of shipping on particulate matter (PM) levels. The sulfur content in ship fuels in SECAs was limited to 1 % by mass in 2010, decreasing to 0.1 % in 2015, while the global average is 2.4 % (IMO, 2010). Less strict sulfur emission controls (0.5 %) will also be implemented worldwide, at the latest in 2025, depending on current negotiations. Ships produced or heavily modified recently must also comply to lower NO_x emissions factors limits, reducing emission factors (in $g\,kWh^{-1}$) by approximately -10% (after 2000) and another -15% (after 2011) compared to ships built before year 2000 (IMO, 2010). Jonson et al. (2015) showed that the creation of the North Sea and Baltic Sea SECAs was effective in reducing current pollution levels in Europe, and that further NO_x and sulfur emission controls in these regions could help to achieve strong health benefits by 2030 by reducing PM levels.

In addition to its impacts on air quality, maritime traffic already contributes to climate change, by increasing the concentrations of greenhouse gases (CO_2, O_3) and aerosols (SO_4, OC, BC) (Capaldo et al., 1999; Endresen et al., 2003). Although ship emissions have competing warming and cooling impacts, the climate effect of ships is currently

dominated by the cooling influence of aerosols, especially sulfate formed from SO_2 emissions (Eyring et al., 2010). In the future, declining global SO_2 emissions due to IMO regulations are expected to change the global climate effect of ships from cooling to warming (Fuglesvedt, 2009; Dalsøren et al., 2013).

5   In addition to their global impacts, shipping emissions are particularly concerning in the Arctic, where they are projected to increase in the future as sea ice declines (for details of future sea ice, see e.g. Stroeve et al., 2011). Decreased sea ice, associated with warmer temperatures, is progressively opening the Arctic region to transit shipping, and projections indicate that new trans-Arctic shipping routes should be available
10 by midcentury (Smith and Stephenson, 2013). Other shipping activities are also predicted to increase, including shipping associated with oil and gas extraction (Peters et al., 2011). Sightseeing cruises have increased significantly during the last decades (Eckhardt et al., 2013), although it is uncertain whether or not this trend will continue. Future Arctic shipping is expected to have important impacts on air quality in a now
15 relatively pristine region (e.g. Granier et al., 2006), and will influence both Arctic and global climate (Dalsøren et al., 2013; Lund et al., 2012). In addition, it has recently been shown that routing international maritime traffic through the Arctic, as opposed to traditional routes through the Suez and Panama canals, will result in warming in the coming century and cooling on the long term, due primarily to the competing effects of
20 reduced SO_2 due to IMO regulations and reduced CO_2 emissions associated with fuel savings (Fuglestvedt et al., 2014).

Although maritime traffic is relatively minor at present in the Arctic compared to global shipping, even a small number of ships can significantly degrade air quality in regions where other anthropogenic emissions are low (Aliabadi et al., 2014; Eckhardt et al.,
25 2013). Dalsøren et al. (2007) and Ødemark et al. (2012) have shown that shipping emissions also influence air quality and climate along the Norwegian and Russian coasts, where current Arctic ship traffic is the largest. Both studies (for years 2000 and 2004 respectively) were based on emission datasets constructed using ship activity data from the AMVER (Automated Mutual-Assistance VEssel Rescue system)

and COADS (Comprehensive Ocean–Atmosphere Data Set) datasets. However, the AMVER dataset is biased towards larger vessels ($> 20\,000$ t) and cargo ships (Endresen et al., 2003), and both datasets have limited coverage in Europe (Miola et al., 2011). More recently, ship emissions using new approaches have been developed that use ship activity data more representative of European maritime traffic, based on the AIS (Automatic Identification System) ship positioning system. These include the STEAM2 (Ship Traffic Emissions Assessment Model version 2) shipping emissions, described in Jalkanen et al. (2012) and an Arctic wide emission inventory described in Winther et al. (2014). To date, quantifying the impacts of Arctic shipping on air quality and climate has also been largely based on global model studies, which are limited in horizontal resolution. In addition, there have not been specific field measurements focused on Arctic shipping that could be used to study the local influence in the European Arctic and to validate model predicted air quality impacts.

In this study, we aim to quantify the impacts of shipping along the Norwegian coast in July 2012, using airborne measurements from the ACCESS (Arctic Climate Change, Economy and Society) aircraft campaign (Roiger et al., 2015). This campaign (Sect. 2) took place in summer 2012 in northern Norway, and was primarily dedicated to the study of local pollution sources in the Arctic, including pollution originating from shipping. ACCESS measurements are combined with two modeling approaches, described in Sect. 3. First, we use the Weather Research and Forecasting (WRF) model to drive the Lagrangian Particle Dispersion Model FLEXPART-WRF run in forward mode to predict the dispersion of ship emissions. FLEXPART-WRF results are used in combination with ACCESS aircraft measurements in Sect. 4 to derive emissions of NO_x and SO_2 for specific ships sampled during ACCESS. The derived emissions are compared to emissions from the STEAM2 model for the same ships. Then, we perform simulations with the WRF-Chem model including STEAM2 ship emissions, in order to examine in Sect. 5 the local and regional impacts of shipping pollution on air quality and shortwave radiative effects along the coast of northern Norway.

Air quality and radiative impacts of Arctic shipping emissions

L. Marelle et al.

Title Page

Abstract	Introduction
Conclusions	References
Tables	Figures

|◄ | ►|
◄ | ►

Back | Close

Full Screen / Esc

Printer-friendly Version

Interactive Discussion

2 The ACCESS aircraft campaign

The ACCESS aircraft campaign took place in July 2012 from Andenes, Norway (69.3° N, 16.1° W); it included characterization of pollution originating from shipping (4 flights) as well as other local Arctic pollution sources (see the ACCESS campaign overview paper for details, Roiger et al., 2015). The aircraft payload included a wide range of instruments measuring meteorological variables and trace gases, described in detail by Roiger et al. (2015). Briefly, O_3 was measured by UV absorption (5 % precision, 0.2 Hz), nitrogen oxide (NO) and nitrogen dioxide (NO_2) by chemilumines-cence and photolytic conversion (10 % precision for NO, 15 % for NO_2, 1 Hz), and SO_2 by Chemical Ionization Ion Trap Mass Spectrometry (20 % precision, 0.3 to 0.5 Hz). Aerosol size distributions between 60 nm and 1 µm were measured using a Ultra-High Sensitivity Aerosol Spectrometer Airborne.

The 4 flights focused on shipping pollution took place on 11, 12, 19 and 25 July 2012 and are shown in Fig. 1a (zoom in on the 11 and 12 July 2012 flights shown in Fig. 1b). The 3 flights on 11, 12 and 25 July 2012 sampled pollution from specific ships (referred to as single-plume flights). During these flights, the research aircraft repeatedly sam-pled relatively fresh emissions from one or more ships during flight legs at constant altitudes, at several distances from the emission source, and in some cases at differ-ent altitudes. In this study, measurements from these single plume flights are used in combination with ship plume dispersion simulations (described in Sects. 3.1 and 4.1) to estimate emissions from individual ships. This method relies on knowing the precise locations of the ships during sampling. Because those locations are not known for the ship emissions sampled on 25 July 2012 flight, emissions are only calculated for the 3 ships targeted during the 11 and 12 July flights (the *Costa Deliziosa*, *Wilson Leer* and *Wilson Nanjing*), and for an additional ship (the *Alaed*) sampled during the 12 July flight, whose location could be retrieved from the STEAM2 shipping emission inven-tory (presented in Sect. 3.3). Table 1 gives more information about these 4 ships, one large cruise ship and three cargo ships. On 11 and 12 July 2012, the research aircraft

Title Page

Abstract | Introduction

Conclusions | References

Tables | Figures

|◀ | ▶|

◀ | ▶

Back | Close

Full Screen / Esc

Printer-friendly Version

Interactive Discussion

sampled fresh ship emissions within the boundary layer, during flight legs at low altitudes (< 200 m). Fresh ship emissions were sampled less than 4 h after emission. In addition to the single plume flights, the 19 July 2012 ACCESS flight targeted aged ship emissions in the marine boundary layer near Trondheim. Data collected during these 4 flights are used to derive emissions from operating ships and to evaluate regional chemical transport simulations investigating the impacts of shipping in northern Norway. Other flights from the ACCESS campaign were not used in this study because their flight objectives biased the measurements towards other emissions sources (e.g. oil platforms in the Norwegian Sea) or because they included limited sampling in the boundary layer (flights north to Svalbard and into the Arctic free troposphere, Roiger et al., 2015).

3   Modeling tools

3.1   FLEXPART-WRF and WRF

Plume dispersion simulations are performed with FLEXPART-WRF for the 4 ships presented in Table 1, in order to estimate their emissions of NO_x and SO_2. FLEXPART-WRF (Brioude et al., 2013) is a version of the Lagrangian particle dispersion model FLEXPART (Stohl et al., 2005), driven by meteorological fields from the mesoscale weather forecasting model WRF (Skamarock et al., 2008). In order to drive FLEXPART-WRF, a meteorological simulation was performed with WRF version 3.5.1, from 4 to 25 July 2012, over the domain presented in Fig. 1a. The domain (15 km × 15 km horizontal resolution with 65 vertical eta levels between the surface and 50 hPa) covers most of northern Norway (∼ 62 to 75° N) and includes the region of all ACCESS flights focused on ship emissions. The first week of the simulation (4 to 10 July included) is used for model spin up. WRF options and parameterizations used in these simulations are shown in Table 2. Meteorological initial and boundary conditions are obtained from the final (FNL) analysis from NCEP (National Centers for Environmental Prediction). The

simulation is also nudged to FNL winds, temperature and humidity every 6 h. This WRF meteorological simulation is referred to as the MET simulation.

Moving ship emissions are represented in the FLEXPART-WRF plume dispersion simulations as moving $2\,m \times 2\,m \times 2\,m$ box sources, whose locations are updated every 10 s along the ship trajectory (routes shown on Fig. 1b). 1000 particles are released every 10 s into these volume sources, representing a constant emission flux with time of an inert tracer. During the ACCESS flights, targeted ships were moving at relatively constant speeds during the $\sim 3\,h$ of the flight, meaning that fuel consumption and emission fluxes are likely to be constant during the flights if environmental conditions (wind speed, waves and currents) were not varying strongly. FLEXPART-WRF takes into account a simple exponential decay using a prescribed lifetime. In our case, the lifetime of NO_x relative to their reaction with OH was estimated using results from WRF-Chem simulations presented in Sect. 3.2. Specifically, we use OH concentrations, temperature and air density from the CTRL3 simulation (see Sects. 3.2 and 5.1). The NO_x lifetime was estimated to be 12 h on 11 July, 5 h on 12 July. The SO_2 lifetime was not taken into account, consistent with the findings of Lee et al. (2011), who reported a lifetime of $\sim 20\,h$ over the mid-Atlantic during summer, which is significantly longer than the ages of plumes measured during ACCESS. The FLEXPART-WRF output consists of particle positions, each associated with a pollutant mass; these particles are mapped onto a 3-D output grid ($600\,m \times 600\,m$, with 18 vertical levels between 0 and 1500 m a.s.l.) to derive fields of volume mixing ratios every minute. Since emissions are assumed to be constant with time and since our simulations only take into account transport processes depending linearly on concentrations, the intensity of these mixing ratio fields also depend linearly on the emission strength chosen for the simulation. Therefore, the model results can be scaled a posteriori to represent any constant emission flux value.

Ship emissions can continue to rise after leaving the exhaust, due to their vertical momentum and buoyancy. This was taken into account in the FLEXPART-WRF simulations by calculating effective injection heights for each targeted ship, using a simple plume rise model (Briggs, 1965). This model takes into account ambient temperature

and wind speed, as well as the volume flow rate and temperature at the ship exhaust, to calculate a plume injection height above the ship stack. Ambient temperature and wind speed values at each ship's position are obtained from the WRF simulation. We use an average of measurements by Lyyranen et al. (1999) and Cooper (2001) as

5 the exhaust temperature of the 4 targeted ships (350 °C). The volume flows at the exhaust are derived for each ship using CO_2 emissions from the STEAM2 ship emission model (STEAM 2 emissions described in Sect. 3.3). Specifically, CO_2 emissions from STEAM2 for the 4 targeted ships are converted to an exhaust gas flow based on the average composition of ship exhaust gases measured by Cooper (2001) and Petzold

10 et al. (2008). Average injection heights, including stack heights and plume rise, are found to be approximately 230 m for the *Costa Deliziosa*, 50 m for the *Wilson Nanjing*, 30 m for the *Wilson Leer* and 65 m for the *Alaed*. In order to estimate the sensitivity of plume dispersion to these calculated injection heights, two other simulations are performed for each ship, where injection heights are decreased and increased by 50 %.

15 Details of the FLEXPART-WRF runs and how they are used to estimate emissions are presented in Sect. 4.

3.2 WRF-Chem

In order to estimate the impacts of shipping on air quality and radiative effects in northern Norway, simulations are performed using the 3-D chemical transport WRF-Chem

20 (Weather Research and Forecasting model, including chemistry, Grell et al., 2005; Fast et al., 2006). WRF-Chem has been used previously by Molders et al. (2010) to quantify the influence of ship emissions on air quality in southern Alaska. Table 2 summarizes all the WRF-Chem options and parameterizations used in the present study, detailed briefly below. The gas phase mechanism is the carbon bond mechanism, version Z

25 (CBM-Z, Zaveri and Peters, 1999). The version of the mechanism used in this study includes dimethylsulfide (DMS) chemistry. Aerosols are represented by the 8 bin sectional MOSAIC (Model for Simulating Aerosol Interactions and Chemistry, Zaveri et al., 2008) mechanism. Aerosol optical properties are calculated by a Mie code within WRF-

Chem, based on the simulated aerosol composition, concentrations and size distributions. These optical properties are linked with the radiation modules (aerosol direct effect), and this interaction also modifies the modeled dynamics and can affect cloud formation (semi-direct effect). The simulations also include cloud/aerosol interactions,

5 representing aerosol activation in clouds, aqueous chemistry for activated aerosols, and wet scavenging within and below clouds. Aerosol activation changes the cloud droplet number concentrations and cloud droplet radii in the Morrison microphysics scheme, thus influencing cloud optical properties (first indirect aerosol effect). Aerosol activation in MOSAIC also influences cloud lifetime by changing precipitation rates

10 (second indirect aerosol effect).

Chemical initial and boundary conditions are taken from the global chemical-transport model MOZART-4 (model for ozone and related chemical tracers version 4, Emmons et al., 2010). In our simulations, the dry deposition routine for trace gases (Wesely, 1989) was modified to improve dry deposition on snow, following the recom-

15 mendations of Ahmadov et al. (2015). The seasonal variation of dry deposition was also updated to include a more detailed dependence of dry deposition parameters on land use, latitude and date, which was already in use in WRF-Chem for the MOZART-4 gas-phase mechanism. Anthropogenic emissions (except ships) are taken from the HTAPv2 (Hemispheric transport of air pollution, version 2) inventory ($0.1° \times 0.1°$ res-

20 olution). Bulk VOCs are speciated using emission profiles for the UK from Murrels et al. (2010). DMS emissions are calculated following the methodology of Nightingale et al. (2000) and Saltzman et al. (1993). The oceanic concentration of DMS in the Norwegian Sea in July, taken from Lana et al. (2011) is $5.8 \times 10^{-6}\,\mathrm{mol\,m^{-3}}$. Other biogenic emissions are calculated online by the MEGAN model (Guenther et al., 2006) within

25 WRF-Chem. Sea salt emissions are also calculated online within WRF-Chem.

The WRF-Chem simulations performed in this study are summarized in Table 3. The CTRL simulation uses the settings and emissions presented above, as well as ship emissions produced by the model STEAM2 (Sect. 3.3). The NOSHIPS simulation is similar to CTRL, but does not include ship emissions. The NOSHIPS and CTRL

simulations are carried out from 4 to 26 July 2012, over the 15 km × 15 km simulation domain presented in Fig. 1a. The CTRL3 and NOSHIPS3 simulations are similar to CTRL and NOSHIPS, but are run on a smaller 3 km × 3 km resolution domain, shown in Fig. 1b, from 10 to 13 July 2012. The CTRL3 and NOSHIPS3 simulations are not nudged to FNL and do not include a subgrid parameterization for cumulus due to their high resolution. Boundary conditions for CTRL3 and NOSHIPS3 are taken from the CTRL and NOSHIPS simulations (using one way nesting within WRF-Chem) and are updated every hour.

The CTRL and CTRL3 simulations are not nudged to the reanalysis fields in the boundary layer, in order to obtain a more realistic boundary layer structure. However, comparison with ACCESS meteorological measurements shows that on 11 July 2012 this leads to an overestimation of marine boundary layer wind speeds (normalized mean bias = +38 %). Since wind speed is one of the most critical parameters in the FLEXPART-WRF simulations, we decided to drive FLEXPART-WRF with the MET simulation instead of using CTRL or CTRL3. In the MET simulation, results are also nudged to FNL in the boundary layer in order to reproduce wind speeds (normalized mean bias of +14 % on 11 July 2012). All CTRL, NOSHIPS, CTRL3, NOSHIPS3 and MET simulations agree well with meteorological measurements during the other ACCESS ship flights.

3.3 High resolution ship emissions from STEAM2

STEAM2 is a high resolution, real time bottom-up shipping emissions model based on AIS positioning data (Jalkanen et al., 2012). STEAM2 calculates fuel consumption for each ship based on its speed, engine type, fuel type, vessel length, and propeller type. The model can also take into account the effect of waves, and distinguishes ships at berth, maneuvering ships and cruising ships. Contributions from weather effects were not included in this study, however. The presence of AIS transmitters is mandatory for large ships (gross tonnage > 300 t) and voluntary for smaller ships.

Title Page

Abstract | Introduction

Conclusions | References

Tables | Figures

|◄ | ►|

◄ | ►

Back | Close

Full Screen / Esc

Printer-friendly Version

Interactive Discussion

Emissions from STEAM2 are compared with emissions derived from measurements for individual ships in Sect. 4. STEAM2 emissions of CO, NO_x, OC, BC (technically elemental carbon in STEAM2), sulfur oxides (SO_x), SO_4, and exhaust ashes are also used in the WRF-Chem CTRL and CTRL3 simulations. SO_x are emitted as SO_2 in WRF-Chem, and NO_x are emitted as 94 % NO, 6 % NO_2 (EPA, 2000). VOC emissions are estimated from STEAM2 CO emissions using a bulk VOC/CO mass ratio of 53.15 %, the ratio used in the Arctic ship inventory from Corbett et al. (2010). STEAM2 emissions were generated on a 5 km × 5 km grid every 30 min for the CTRL simulation, and on a 1 km × 1 km grid every 15 min for the CTRL3 simulation, and were regridded on the WRF-Chem simulation grids. Shipping emissions of NO_x, SO_2, black carbon, and organic carbon are presented in Fig. 2 for the 15 km × 15 km simulation domain (emissions totals during the simulation period are indicated within the figure panels). For comparison, the HTAPv2 emissions (without shipping emissions) are also shown. Ship emissions are, on average, located in main shipping lanes along the Norwegian coastline. However, they also include less traveled routes, which are apparent closer to shore. Other anthropogenic emissions are mainly located along the Norwegian coast (mostly in southern Norway) or farther inland and to the south in Sweden and Finland. Over the whole domain, NO_x and OC emissions from shipping are approximately one third of total anthropogenic NO_x and OC emissions, but represent a lower proportion of anthropogenic SO_2 and BC emissions (5 and 10 %, respectively). However, other anthropogenic emissions are not co-located with shipping emissions, which represent an important source further north along the coast, as many ships are in transit between European ports and Murmansk in Russia. Very strong SO_2 emissions in Russia are included in the model domain, associated with smelting activities that occur on the Russian Kola Peninsula (Fig. 2d, Virkkula et al., 1997; Prank et al., 2010).

STEAM2 emissions are based on AIS signals that are transmitted to base stations on shore that have a limited range of 50–90 km, which explains why the emissions presented on Fig. 2 only represent near-shore traffic. In addition, our study is focused on shipping emissions in northern Norway, therefore STEAM2 emissions were only gener-

ated along the Norwegian coast. As a result, ship emissions in the northern Baltic and along the northwestern Russian coast are not included in this study. However, these missing shipping emissions are much lower than other anthropogenic sources inside the model domain. Ship emissions are injected in altitude using the plume rise model

5 presented in Sect. 3.1 in the CTRL and CTRL3 simulations. Stack height and exhaust fluxes are unknown for most of the ships present in the STEAM2 emissions, which were not specifically targeted during ACCESS. For these ships, exhaust parameters for the *Wilson Leer* (~ 6000 gross tonnage) are used as a compromise between the smaller fishing ships (~ 40 % of Arctic shipping emissions, Winther et al., 2014), and larger

10 ships like the ones targeted during ACCESS. In the CTRL3 simulation, the 4 ships targeted during ACCESS are usually alone in a 3 km × 3 km grid cell, which enabled us to treat these ships separately and to inject them in altitude using their individual exhaust parameters (Sect. 3.1). In the CTRL simulation, there are usually several ships in the same 15 km × 15 km grid cell, and the 4 targeted ships were treated in the same way

15 together with all unidentified ships, using the exhaust parameters of the *Wilson Leer* and local meteorological conditions to estimate injection heights.

Primary aerosol emissions from STEAM2 (BC, OC, SO_4 and ash) are distributed into the 8 MOSAIC aerosol bins in WRF-Chem, according to the mass size distribution measured in the exhaust of ships equipped with medium-speed diesel engines

20 by Lyyranen et al. (1999). The submicron mode of this measured distribution is used to distribute primary BC, OC and $SO_4^=$, while the coarse mode is used to distribute exhaust ash particles (represented as "other inorganics" in MOSAIC).

4 Ship emission evaluation

In this section, emissions of NO_x and SO_2 are determined for the 4 ships sampled dur-

25 ing ACCESS flights (shown in Table 1). First, we compare airborne measurements in ship plumes and concentrations predicted by FLEXPART-WRF plume dispersion simulations. In order to derive emission fluxes, good agreement between measured and

modeled plume locations is required (discussed in Sect. 4.1). The methods, derived emissions values for the 4 ships, and comparison with STEAM2 emissions, are presented in Sect. 4.2.

4.1 Ship plume representation in FLEXPART-WRF and comparison with airborne measurements

FLEXPART-WRF plume dispersion simulations driven by the MET simulation are performed for the 4 ships sampled during ACCESS (Sect. 3.1). The MET simulation agrees well with airborne meteorological measurements on both days in terms of wind direction (mean bias of $-16°$ on 11 July, $+6°$ on 12 July) and wind speed (normalized mean bias of $+14\%$ on 11 July, -17% on 12 July). Figure 3 shows the comparison between maps of the measured NO_x and plume locations predicted by FLEXPART-WRF. This figure also shows the typical meandering pattern of the plane during ACCESS, measuring the same ship plumes several times as they age, while moving further away from the ship (Roiger et al., 2015). Modeled and measured plume locations agree well for all ships. *Wilson Leer* and *Costa Deliziosa* plumes were sampled during two different runs at two altitudes on 11 July 2012, and presented in Fig. 3a and b ($z = 49$ m) and Fig. 3c and d ($z = 165$ m). During the second altitude level on 11 July (Fig. 3c and d) the *Wilson Leer* was farther south and the *Costa Deliziosa* had moved further north. Therefore, the plumes are farther apart than during the first pass at 49 m. On 12 July 2012, the aircraft targeted emissions from the *Wilson Nanjing* ship (Fig. 3e and f), but also sampled the plume of another ship, the *Alaed*. This last ship was identified during the post-campaign analysis, and we were able to extract its location and emissions from the STEAM2 inventory in order to perform the plume dispersion simulations shown here. The NO_x and FLEXPART-WRF predicted plume locations are again in good agreement for both ships.

Modeled air tracer mixing ratios are interpolated in space and time to the aircraft location, and compared with airborne NO_x and SO_2 measurements (Fig. 4). Each peak in Fig. 4 corresponds to the aircraft crossing the ship plume once during the meander-

ing pattern before turning around for an additional plume crossing. As expected from the comparison shown in Fig. 3, modeled peaks are co-located with measured peaks in Fig. 4. The model is also able to reproduce the gradual decrease of concentrations measured in the plume of the *Wilson Nanjing* on Fig. 4c–e, as the plane flies further away from the ship and the plume gets more dispersed. These peak concentrations vary less for the measured and modeled plume of the *Costa Deliziosa* (Fig. 4a and b). Measured plumes are less concentrated for the *Wilson Leer* since it is a smaller vessel, and for the *Alaed* because its emissions were sampled further away from their source.

4.2 Ship emission derivation and comparison with STEAM2

In this section, we describe the method for deriving ship emissions of NO_x and SO_2 using FLEXPART-WRF and measurements. This method relies on the fact that in the FLEXPART-WRF simulations presented in Sect. 3.1, there is a linear relationship between the constant emission flux of tracer chosen for the simulation and the tracer concentrations in the modeled plume. In our simulations, this constant emission flux is picked at $E = 0.1\,\mathrm{kg\,s^{-1}}$ and is identical for all ships. This initial value E is scaled for each ship by the ratio of the measured and modeled areas of the peaks in concentration corresponding to plume crossings, as shown in Fig. 4. Equation (1) shows how SO_2 emissions are derived by this method.

$$E_i = E \times \frac{\int_{t_i^{\mathrm{begin}}}^{t_i^{\mathrm{end}}} (SO_2(t) - SO_2\mathrm{background})\,\mathrm{d}t}{\int_{t_i^{\mathrm{begin}}}^{t_i^{\mathrm{end}}} \mathrm{Tracer}(t)\mathrm{d}t} \times \frac{M_{SO_2}}{M_{\mathrm{air}}} \tag{1}$$

In Eq. (1), $SO_2(t)$ is the measured SO_2 mixing ratio (ppt), $SO_2\mathrm{background}$ is the background SO_2 mixing ratio for each peak, $\mathrm{Tracer}(t)$ is the modeled tracer mixing ratio interpolated along the ACCESS flight track (ppt), t_i^{begin} and t_i^{end} are the beginning and end time of peak i (modeled or measured, in s) and M_{SO_2} and M_{air} are the molar

masses of SO_2 and air ($kg\,m^{-3}$). This method produces a different E_i SO_2 emission flux value ($kg\,s^{-1}$) for each of the $i = 1$ to N peaks corresponding to all the crossings of a single ship plume by the aircraft. These N different estimates are averaged together to reduce the uncertainty in the estimated SO_2 emissions. A similar approach is used
5   to estimate NO_x emissions.

In order to reduce sensitivity to the calculated emission injection heights, FLEXPART-WRF peaks that are sensitive to a ±50 % change in injection height are excluded from the analysis. Results are considered sensitive to injection heights if the peak area in tracer concentration changes by more than 50 % in the injection height sensitivity runs.
10 Using a lower threshold of 25 % alters the final emission estimates by less than 6 %. Peaks sensitive to the calculated injection height typically correspond to samplings close to the ship, where the plumes are narrow. An intense SO_2 peak most likely associated with the *Costa Deliziosa* and sampled around 17:25 UTC on 11 July 2012 is also excluded from the calculations, because this large increase in SO_2 in an older, diluted
15 part of the ship plume suggests contamination from another source. SO_2 emissions are not determined for the *Wilson Leer* and the *Alaed*, since SO_2 measurements in their plumes are too low to be distinguished from the background variability. For the same reason, only the higher SO_2 peaks (4 peaks > 1 ppb) were used to derive emissions for the *Wilson Nanjing*. The number of peaks used to derive emissions for each ship is
20 $N = 13$ for the *Costa Deliziosa*, $N = 4$ for the *Wilson Leer*, $N = 8$ for the *Wilson Nanjing* ($N = 4$ for SO_2) and $N = 5$ for the *Alaed*.

The derived emissions of NO_x (equivalent NO_2 mass flux in $kg\,day^{-1}$) and SO_2 are given in Table 4. The emissions extracted from the STEAM2 inventory for the same ships during the same time period are also shown. STEAM2 SO_2 emissions are higher
25 than the value derived for the *Costa Deliziosa*, and lower than the value derived for the *Wilson Nanjing*, but NO_x emissions from STEAM2 are higher than our calculations for all ships. In STEAM2, the NO_x emission factor is assigned according to IMO MARPOL (marine pollution) Annex VI requirements (IMO, 2008) and engine revolutions per minute (RPM); but all engines subject to these limits must emit less NO_x than this re-

Air quality and radiative impacts of Arctic shipping emissions

L. Marelle et al.

Title Page

Abstract | Introduction

Conclusions | References

Tables | Figures

|◄ | ►|

◄ | ►

Back | Close

Full Screen / Esc

Printer-friendly Version

Interactive Discussion

quired value. For the *Wilson Leer*, two calculated values are reported: one calculated by averaging the estimates from the 4 measured peaks, and one value where an outlier value was removed before calculating the average. During the 11 July flight, the *Wilson Leer* was traveling south at an average speed of $4.5\,\mathrm{m\,s^{-1}}$, with relatively slow tailwinds of $5.5\,\mathrm{m\,s^{-1}}$. Because of this, the dispersion of this ship's plume on this day could be sensitive to small changes in modeled wind speeds, and calculated emissions are less certain.

The most important difference between the inventory NO_x and our estimates is $\sim 150\,\%$ for the *Costa Deliziosa*. Reasons for large discrepancy in predicted and measured NO_x emissions of *Costa Deliziosa* were investigated in more detail. A complete technical description of *Costa Deliziosa* was not available, but her sister vessel *Costa Luminosa* was described at length recently (RINA, 2010). The details of *Costa Luminosa* and *Costa Deliziosa* are practically identical and allow in-depth analysis of emission modeling. With complete technical data, the STEAM2 SO_x and NO_x emissions of *Costa Deliziosa* were estimated to be 2684 and $5243\,\mathrm{kg\,day^{-1}}$, respectively, whereas our derived estimates indicate 2399 and $2728\,\mathrm{kg\,day^{-1}}$ (difference of $+12\,\%$ for SO_x and $+92\,\%$ for NO_x). The good agreement for SO_x indicates that the power prediction at vessel speed reported in AIS and associated fuel flow is well predicted by STEAM2, but emissions of NO_x are twice as high as the value derived from measurements. In case of *Costa Deliziosa*, the NO_x emission factor of $10.5\,\mathrm{g\,kWh^{-1}}$ for a Tier II compliant vessel with 500 RPM engine is assumed by STEAM2. Based on the measurements-derived value, a NO_x emission factor of $5.5\,\mathrm{g\,kWh^{-1}}$ would be necessary, which is well below the Tier II requirements. It was reported recently (IPCO, 2015), that NO_x emission reduction technology was installed on *Costa Deliziosa*, but it is unclear whether this technology was in place during the airborne measurement campaign in 2012.

The case of *Costa Deliziosa* underlines the need for accurate and up-to-date technical data for ships when bottom-up emission inventories are constructed. It also necessitates the inclusion of the effect of emission abatement technologies in ship emission inventories. Furthermore, model predictions for individual vessels are complicated by

Air quality and radiative impacts of Arctic shipping emissions

L. Marelle et al.

external contributions, like weather and sea currents, affecting vessel performance. A recent study by Beecken et al. (2014) compared STEAM2 NO_x, SO_2 and PM emission factors to estimates based on airborne measurements for $\sim$ 300 ships in the Baltic Sea and found, on average, no strong bias in STEAM2 predictions of NO_x. In Beecken et al. (2014) the emission factors of SOx and PM were shown to deviate from measurements mainly because of the differences in assumed and measured fuel sulfur content. Regardless of the differences, regional emission inventories generated by STEAM2 can describe the geographical distribution of ship emissions accurately. The results presented later in Sect. 5.1 indicate that this is also likely true in the Norwegian Sea during ACCESS, despite the uncertainties for individual ships.

4.3 Comparison of STEAM2 to other shipping emission inventories for northern Norway

We compare in Table 5 the July emission totals for NO_x, SO_2, BC, OC and $SO_4^=$ in northern Norway (latitudes 60.6 to 73° N, longitudes 0 to 31° W) for STEAM2 and 4 other shipping emission inventories used in previous studies investigating shipping impacts in the Arctic. We include emissions from the Winther et al. (2014), Dalsøren et al. (2009, 2007) and Corbett et al. (2010) inventories. The highest shipping emissions in the region of northern Norway are found in the STEAM2 and Winther et al. (2014) inventories, which are both based on 2012 AIS ship activity data (see Sect. 3.3 for a description of the methodology used for STEAM2). We note that, except for OC, the emissions are higher in the Winther et al. (2014) inventory because of the larger geographical coverage: Winther et al. (2014) used both ground based and satellite retrieved AIS signals, whereas the current study is restricted to data received by ground based AIS stations (capturing ships within 50 to 90 km of the Norwegian coastline). Despite lower coverage, the horizontal and temporal resolutions are better described in land based AIS networks than satellite AIS data. The terrestrial AIS data used in this study is thus more comparable to the spatial extent and temporal resolution of the measurements collected close to the Norwegian coast. STEAM2 is the only in-

ventory including sulfate emissions, which account for SO_2 to $SO_4^=$ conversion in the ship exhaust. Ship emissions from Dalsøren et al. (2009) and Corbett et al. (2010) are based on ship activity data from 2004, when marine traffic was lower than in 2012. Furthermore, the gridded inventory from Corbett et al. (2010) does not include emissions from fishing ships, which represent close to 40 % of Arctic shipping emissions (Winther et al., 2014). These emissions could not be precisely distributed geospatially using earlier methodologies, since fishing ships do not typically follow a simple course (Corbett et al., 2010). Dalsøren et al. (2007) emissions for coastal shipping in Norwegian waters are estimated based on Norwegian shipping statistics for the year 2000, and contain higher NO_x, BC and OC emissions, but less SO_2, than the 2004 inventories. This comparison indicates that earlier ship emission inventories usually contain lower emissions in this region, which can be explained by the current growth in shipping traffic in northern Norway. This means that up-to-date emissions are required in order to assess the current impacts of shipping in this region.

5 Modeling the impacts of ship emissions along the Norwegian coast

In this section, WRF-Chem using STEAM2 ship emissions is employed to study the influence of ship pollution on atmospheric composition along the Norwegian coast, at both the local and regional scale. As shown in Fig. 4, shipping pollution measured during ACCESS is inhomogeneous, with sharp NO_x and SO_2 peaks in thin ship plumes, emitted into relatively clean background concentrations. The measured concentrations are on spatial scales that can only be reproduced using very high-resolution WRF-Chem simulations (a few kms of horizontal resolution), but such simulations can only be performed for short periods and over small domains. Therefore, high-resolution simulations cannot be used to estimate the regional impacts of shipping emissions. In order to bridge the scale between measurements and model runs that can be used to make conclusions about the regional impacts of shipping pollution, we compare in Sect. 5.1 WRF-Chem simulations using STEAM2 ship emissions, at 3 km × 3 km resolu-

Air quality and radiative impacts of Arctic shipping emissions

L. Marelle et al.

tion (CTRL3) and at $15\,\text{km} \times 15\,\text{km}$ resolution (CTRL). Specifically, we show in Sect. 5.1 that both the CTRL3 and CTRL simulations reproduce the average regional influence of ships on NO_x, O_3 and SO_2, compared to ACCESS measurements. In Sect. 5.2 we use the CTRL simulation to quantify the regional contribution of ships to surface pollution and shortwave radiative fluxes in northern Norway.

5.1 Local impacts of ship emissions and influence of model resolution

It is well known that ship plumes contain fine scale features that cannot be captured by most regional or global chemical transport models. This fine plume structure influences the processing of ship emissions, including O_3 and aerosol formation, which are non-linear processes that largely depend on the concentration of species inside the plume. Some models take into account the influence of the instantaneous mixing of ship emissions in the model grid box by including corrections to the O_3 production and destruction rates (Huszar et al., 2010) or take into account plume ageing before dilution by using corrections based on plume chemistry models (Vinken et al., 2011). Here, we take an alternative approach by running the model at a sufficient resolution to distinguish individual ships in the Norwegian Sea (CTRL3 run at $3\,\text{km} \times 3\,\text{km}$ resolution), and at a lower resolution (CTRL run at $15\,\text{km} \times 15\,\text{km}$ resolution). The CTRL and CTRL3 simulations (see Table 3) are compared to evaluate if nonlinear effects are important in this case. We also evaluate the ability of WRF-Chem simulations with STEAM2 emissions to distinguish individual ship plumes and to predict their composition.

WRF-Chem results from CTRL and CTRL3 for surface (~ 0 to $30\,\text{m}$) NO_x and O_3 are shown in Fig. 5. On 11 and 12 July, the Falcon 20 specifically targeted plumes from the *Wilson Leer*, *Costa Deliziosa*, *Wilson Nanjing* and, in addition, sampled emissions from the *Alaed*, identified later during the post-campaign analysis (see Fig. 3). All these ships are individually present in the STEAM2 emissions inventory (see Sect. 4 and Table 4). Emissions from these ships as well as from other vessels traveling in that area are clearly resolved in the CTRL3 model results for NO_x (Fig. 5a and e). Ship NO_x emissions are smoothed out in the CTRL run, seen in Fig. 5b and f, and the

Title Page

Abstract | Introduction

Conclusions | References

Tables | Figures

◄ | ►|

◄ | ►

Back | Close

Full Screen / Esc

Printer-friendly Version

Interactive Discussion

individual ship plumes cannot be clearly distinguished in the NO_x surface concentrations. The predicted surface O_3 concentrations are shown in Fig. 5c, d, g, and h. On the 11 and 12 July 2012, titration of O_3 by NO from fresh ship emissions can be identified in Fig. 5c and g for the 3 km run (areas indicated by black arrows on Fig. 5c and

5   g). However, evidence for O_3 titration quickly disappears away from the fresh emissions sources. In contrast, O_3 titration is not apparent in the CTRL run. However, NO_x and O_3 patterns and average surface concentrations are very similar. This is illustrated in the lower panels, showing 2-day averaged NO_x and O_3 enhancements due to ships in the CTRL3 (CTRL3 – NOSHIPS3) and CTRL (CTRL – NOSHIPS) simulations. The results

10   show that changing the horizontal resolution from 3 km × 3 km (1 km × 1 km emissions, 15 min emissions injection) to 15 km × 15 km (5 km × 5 km emissions, 1 h emissions injection) does not have a large influence on the domain-wide average NO_x (−3.2 %) or O_3 (+4.2 %) enhancements due to ships. This is in agreement with earlier results by Cohan et al. (2006), who showed that regional model simulations at similar resolu-

15   tions (12 km) were sufficient to reproduce the average O_3 response. Results by Vinken et al. (2011) suggest that simulations at a lower resolution more typical of global models ($2° × 2.5°$) would lead to an overestimation of O_3 production from ships in this region by 1 to 2 ppbv. The influence of model resolution on surface aerosol concentrations is also moderate, and PM_{10} due to ships are 15 % lower on average in CTRL than in

20   CTRL3 (not shown here).

To further investigate the ability of these different model runs to represent single ship plumes, we compare measured NO_x and O_3 along the flight track on 11 July 2012 with WRF-Chem predictions (Fig. 6). Large enhancements of NO_x are seen during plume crossings in measurements, as already noted in Sect. 4. For comparison with WRF-

25   Chem, we have averaged the measured data using a 56 s running average, equivalent to the aircraft crossing 6 km (2 model grid cells) at its average speed during this flight ($107\,\mathrm{m\,s^{-1}}$). Using a running average takes into account plume dilution in grid cells, as well as additional smoothing introduced when modeled results are spatially interpolated onto the flight track. The CTRL3 simulation captures both the width and magnitude of

NO$_x$ peaks, suggesting that the individual plumes are correctly represented in space and time. In contrast, the CTRL run has wider NO$_x$ peaks and lower peak heights, because of dilution in larger grids. Both simulations have a tendency to overestimate NO$_x$ in ship plumes, which is in agreement with the results shown in Table 4, indi-
5 cating that STEAM2 NO$_x$ emissions are overestimated for the ships targeted during ACCESS. Figure 6b shows O$_3$ during the same flight. The CTRL3 simulation reproduces the ozone variability better than the CTRL run, but both runs perform relatively well on average (mean bias $= -3$ ppbv during the constant altitude legs). Both measurements and CTRL3 results show evidence of O$_3$ titration in the most concentrated
10 NO$_x$ plumes, where ozone is 1.5 to 3 ppbv lower than out of the plumes. However, precise quantification of this titration is difficult because these values are the same order of magnitude as the spatial variability of O$_3$ outside of the plumes. O$_3$ titration is not apparent in the CTRL run.

In order to evaluate modeled aerosols in ship plumes, modeled aerosols are eval-
15 uated using size distributions measured during the 11 July 2012 flight. Size distributions are integrated to estimate submicron aerosol mass (PM$_1$), assuming a density of 1700 kg m^{-3} and spherical particles. This indicates that observed PM$_1$ enhancements in plumes ($\sim$ 0.1 to 0.5 µg m^{-3}) are relatively low compared to background PM$_1$ ($\sim$ 0.7 to 1.1 µg m^{-3}), because of the presence of high sea salt concentrations in the marine
20 boundary layer (54 % of the modeled background PM$_1$ during ship plume sampling is sea salt in NOSHIPS3). Because of this, comparing modeled and observed in-plume PM$_1$ directly would be mostly representative of background aerosols, especially sea salt, which is not the focus of this paper. Figure 7 shows the comparison between modeled and measured enhancements in PM$_1$ in the plume of the *Costa Deliziosa*
25 (11 July 2012), removing from the model and measurements the contribution from sea salt and other aerosols not associated with shipping. Similarly to Fig. 6, a 56 s moving average was applied to the measurement (representing plume dilution in the model grid). This comparison indicates a generally good agreement between modeled and measured PM$_1$ enhancements in ship plumes. There is a discrepancy between the

model and the measurements for the first 2 PM_1 plumes measured close to the ships (around 16:05 UTC), which could be an artifact of the limited resolution of this simulation (3 km). If these peaks are excluded, the model slightly overestimates peak PM_1 enhancements in ship plumes (+26 %). Since this enhancement is modeled as 80 %

5 $SO_4^=$, this overestimation can be linked to the +37 % overestimation of SO_2 emissions for the *Costa Deliziosa* in STEAM2 (see Table 4).

Analysis of O_3 maps, average surface enhancements due to ships (Fig. 5) and analysis of model results along flight tracks (Fig. 6) show that both runs capture the NO_x and O_3 concentrations in this region reasonably well. Furthermore, Fig. 7 shows that

10 PM_1 enhancements in ship plumes are well reproduced in the CTRL3 simulation, and we found that PM_{10} production from ships over the simulation domain was not very sensitive to resolution. This suggests that the CTRL simulation is sufficient to assess the impacts of ship emissions at a larger scale during July 2012. This is investigated further by comparing modeled NO_x, SO_2 and O_3 in the CTRL and NOSHIPS simu-

15 lations with the average vertical profiles (100–1500 m) measured during 4 ACCESS flights from 11 to 25 July 2012 (flights shown in Fig. 1a); this comparison is shown in Fig. 8. Modeled vertical profiles of $PM_{2.5}$ are also shown in Fig. 8. This comparison allows us to estimate how well CTRL represents the average impact of shipping over a larger area and a longer period.

20 Figure 8 shows that the NOSHIPS simulation significantly underestimates NO_x and SO_2, and moderately underestimates O_3 along the ACCESS flights, indicating that ship emissions are needed to improve the agreement between the model and observations. In the CTRL simulation, NO_x, SO_2 and O_3 vertical structure and concentrations are generally well reproduced, with normalized mean biases of +6.9, −10.7 and −7.5 %

25 respectively. Correlations between modeled (CTRL) and measured profiles are significant for NO_x and O_3 (r^2 = 0.94 and 0.95). The correlation is lower between measured and modeled SO_2 (r^2 = 0.52) but it is improved compared to the NOSHIPS simulation (r^2 = 0.35). Ships have the largest influence on NO_x and SO_2 profiles, a moderate influence on O_3 and do not strongly influence $PM_{2.5}$ profiles along the ACCESS flights.

NO$_x$ concentrations are overestimated in the parts of the profile strongly influenced by shipping emissions. This is in agreement with the findings of Sect. 4.2, showing that STEAM2 NO$_x$ emissions were overestimated for the ships sampled during ACCESS. However, the CTRL simulation performs well on average, suggesting that the STEAM2 inventory is able to represent the average emissions from ships along the northern Norwegian coast during the study period. The bias found for SO$_2$ is especially low compared to the results presented in the multi-model study of Eyring et al. (2007), which showed that global models significantly underestimated SO$_2$ in the polluted marine boundary layer in July. Since aerosols from ships contain mostly secondary sulfate formed from SO$_2$ oxidation, the validation of modeled SO$_2$ presented in Fig. 8 gives some confidence in our results compared to earlier studies investigating the air quality and radiative impacts of shipping aerosols. We therefore use the 15 km × 15 km CTRL run for further analysis of the regional influence of ships on pollution and the shortwave radiative effect in this region in Sect. 5.2.

5.2 Regional influence of ship emissions in July 2012

5.2.1 Surface air pollution from ship emissions in northern Norway

The regional scale impacts of ships on surface atmospheric composition in northern Norway are estimated by calculating the 15 day (00:00 UTC, 11 July 2012 to 00:00 UTC, 26 July 2012) average difference between the CTRL and NOSHIPS simulations. Figure 9 shows maps of these anomalies at the surface, for NO$_x$, O$_3$ PM$_{2.5}$ and BC. Ship emissions have the largest influence on surface NO$_x$ concentrations, with 75 to 100 % increases along the coast. This leads to average O$_3$ increases from shipping of ∼ 6 % (∼ 1.5 ppb) in the coastal regions, with slightly lower enhancements (∼ 1 ppb, ∼ 4 %,) further inland over Sweden.

Dalsøren et al. (2007) studied the impact of maritime traffic in northern Norway in summer using ship emission estimates for the year 2000. They found, for July 2000, a 1 to 1.5 % increase in surface O$_3$ from coastal shipping in Norwegian waters. How-

ever, unlike the present study, the estimate of Dalsoren et al. (2007) did not include the impact of international transit shipping along the Norwegian coast. Our estimated impact on O_3 in this region (6 % and 1.5 ppb increase) is about half of the one determined by Ødemark et al. (2012) (12 % and 3 ppb), for the total Arctic fleet in the summer (JAS) 2004, using ship emissions for the year 2004 from Dalsøren et al. (2009). It is important to note that we expect lower impacts of shipping in studies based on earlier years, because of the continued growth of shipping emissions along the Norwegian coast (as discussed in Sect. 4.3, see also Table 5). However, stronger or lower emissions do not seem to completely explain the different modeled impacts. Ødemark et al. (2012) found that Arctic ships had a strong influence on surface O_3 in northern Norway for relatively low 2004 shipping emissions. This could be explained by the different processes included in both models, or by different meteorological situations in the two studies based on two different meteorological years (2004 and 2012). However, it is also likely that the higher O_3 in the Ødemark et al. (2012) study could be caused, in part, by nonlinear effects associated with global models running at low resolutions. For example Vinken et al. (2011) estimated that instant dilution of shipping NO_x emissions in $2° \times 2.5°$ model grids leads to a 1 to 2 ppb overestimation in ozone in the Norwegian and Barents seas during July 2005. This effect could explain a large part of the difference in O_3 enhancements from shipping between the simulations of Ødemark et al. (2012) ($2.8° \times 2.8°$ resolution) and the simulations presented in this paper (15 km × 15 km resolution).

The impact on $PM_{2.5}$ of ships in northern Norway, also shown in Fig. 9., is relatively modest during this period, up to 0.75 µg m^{-3}. However, these values correspond to an important relative increase of ∼ 10 % over inland Norway and Sweden because of the low background $PM_{2.5}$ in this region. Over the sea surface, the relative effect of ship emissions is quite low because of higher sea salt aerosol background. Aliabadi et al. (2014) have observed similar increases in $PM_{2.5}$ (0.5 to 1.9 µg m^{-3}) in air masses influenced by shipping pollution in the remote Canadian Arctic. In spite of the higher traffic in northern Norway, we find lower values because results in Fig. 9 are smoothed

by the 15 day average. Impacts on surface BC concentrations are quite large, reaching up to 50 %. We note that Eckhardt et al. (2013) have found enhancements in summertime equivalent BC of 11 % in Svalbard from cruise ships alone. As expected, absolute BC enhancements in our simulations are higher in the southern part of the domain, where ship emissions are the strongest. Given its short lifetime, BC is not efficiently transported away from the source region.

5.2.2 Shortwave radiative effect of ship emissions in northern Norway

The climate effect of ship emissions is mostly due to aerosols, especially sulfate, which cool the climate through their direct and indirect effects (Capaldo et al., 1999). However, large uncertainties still exist concerning the magnitude of the aerosol indirect effects (Boucher et al., 2013). In this section, we determine the total shortwave radiative effect of ships by calculating the difference between the top-of-atmosphere (TOA) upwards shortwave (0.125 to 10 µm wavelengths) radiative flux in the CTRL and the NOSHIPS simulations. Since the CTRL and NOSHIPS simulations take into account aerosol/radiation interactions and their feedbacks (the so-called direct and semi-direct effects) as well as cloud/aerosol interactions (indirect effects), this quantity represents the sum of modeled direct, semi-direct and indirect effects from aerosols associated with ship emissions. Yang et al. (2011) and Saide et al. (2012) showed that including cloud aerosol couplings in WRF-Chem improved significantly the representation of simulated clouds, indicating that the indirect effect was relatively well simulated using CBM-Z/MOSAIC chemistry within WRF-Chem.

The shortwave radiative effect at TOA of in-domain ship emissions is $-1.77\,\mathrm{W\,m^{-2}}$ (15 day average). Averaged over the surface of the Earth, this value corresponds to an equivalent shortwave radiative effect at the global scale at TOA of $-9.3\,\mathrm{mW\,m^{-2}}$. It is similar to the estimate by Ødemark et al. (2012), who found a direct and indirect shortwave effect of aerosols from Arctic-wide shipping in July 2004 of $-10.4\,\mathrm{mW\,m^{-2}}$. However, since the present study only represents the effect of shipping along the Norwegian coast, this implies that current ship emissions in northern Norway have a stronger ef-

fect in this study than in Ødemark et al. (2012), which was based on ship emissions from Dalsøren et al. (2009) corresponding to 24 % less SO_2 emissions than STEAM2. Higher emissions in our simulations could partly explain the stronger local shortwave effect of Arctic ships, since this effect is mostly associated with the direct and indi-
5 rect effect of sulfate aerosols. However, the total sulfate column due to ship emissions in our study is 100 to 200 μg m^{-2} along the Norwegian coast, half of the value (250 to 300 μg m^{-2}) found by Odemark et al. (2012). This means that the stronger forcing found here is not due to increased sulfate concentrations from larger emissions, but to the way aerosol/cloud interactions are treated in both models: the indirect aerosol
10 effect was calculated by Ødemark et al. (2012) based on parameterizations of the relationship between clouds droplet numbers and aerosol mass, whereas the MOSAIC aerosol module used in this study explicitly treats aerosol activation within clouds and the impacts on cloud properties (Yang et al., 2011).

6   Conclusions

15 The focus of this work, linking modeling and measurements, is to better quantify regional atmospheric impacts of ships in northern Norway in July 2012. The study relies on measurements from the ACCESS aircraft campaign, emissions evaluation and regional modeling in order to evaluate both individual ship plumes and their regional scale effects. STEAM2 emissions, which represent individual ships based on high-resolution
20 AIS ship positioning data, are compared with emissions for specific ships derived from measurements and plume dispersion modeling using FLEXPART-WRF. Regional WRF-Chem simulations run with and without ship emissions are performed at two different resolutions to quantify the surface air quality changes and radiative effects from ship emissions in northern Norway in July 2012. The most important conclusions from our
25 study are:

1. *Validation of the STEAM2 emissions* – Emissions of NO$_x$ and SO_2 are determined for individual ships, by comparing airborne measurements with plume dispersion

modeling results. These calculated emissions are compared with bottom-up emissions determined for the same ships by the STEAM2 emission model. Results show that STEAM2 overestimates NO_x emissions for the 4 ships sampled during ACCESS. SO_2 emissions are also determined for two ships. Large biases are possible for individual ships in STEAM2, especially for ships for which there is incomplete technical data or where emission reduction techniques have been employed. Nevertheless, regional WRF-Chem simulations using STEAM2 emissions agree well on average with ACCESS airborne measurements of NO_x, SO_2 and O_3 during ship flights, indicating that STEAM2 represents reasonably well average emissions from shipping along the coast of northern Norway in summer 2012.

2. *Regional model representation of ship plumes and their local scale influence* – WRF-Chem runs including shipping emissions from STEAM2 are performed at $15\,km \times 15\,km$ and $3\,km \times 3\,km$ horizontal resolutions, and compared with airborne measurements of NO_x and ozone. The high-resolution simulation is better at reproducing measured NO_x peaks and suggests some ozone titration in ship plumes, but the NO_x and ozone enhancements due to ships in both simulations are within less than 5 % of each other when averaged over the whole domain and simulation period. The $3\,km \times 3\,km$ simulation also reproduces observed PM_1 enhancements in ship plumes. Surface PM_{10} enhancements due to ships are 15 % higher in the $3\,km \times 3\,km$ resolution simulation.

3. *Average influence of ship pollution in July 2012* – The difference between runs with and without ship emissions are compared with campaign average profiles (excluding flights focused on oil platforms, smelters, and biomass burning emissions from outside the simulation domain). Including STEAM2 emissions reduces the mean bias between measured and modeled trace gases NO_x, SO_2 and O_3. At the surface, ship emissions enhance 15 day averaged concentrations along the Norwegian coast by approximately 80 % for NO_x, 5 % for O_3, 40 % for BC

and 10 % for $PM_{2.5}$ suggesting that these emissions are already having an impact on atmospheric composition in this region. Regional model results presented in this study predict lower ozone production from ships compared to certain earlier studies using global models. However, it is known that global models run at low resolution tend to overestimate ozone production (underestimate ozone titration) from fresh ship emissions because of nonlinearities introduced when diluting concentrated emissions from ships into coarse model grid cells.

4. *Influence on the radiative budget* – Northern Norwegian ship emissions contribute $-9.3 \, \mathrm{m W m^{-2}}$ to the global shortwave radiative budget of ship emissions, including semi-direct and indirect effects. These results are more significant than found previously in a study using a global model that did not explicitly resolve aerosol activation in clouds. This suggests that global models may be underestimating the radiative impacts of shipping in this region.

Our study shows that local shipping emissions along the northern Norwegian coast already have a significant influence on regional air quality and aerosol shortwave radiative effects. As Arctic shipping continues to grow and new regulations are implemented, the magnitude of these impacts is expected to change. Due to the limited region (northern Norway) and the short time scale (15 days) considered here, it is not possible to assess the radiative effect of other climate forcers associated with shipping in northern Norway, including O_3 and CO_2, which global model studies have suggested are also significant (Dalsøren et al., 2013; Ødemark et al., 2012). However, since shipping emissions are highly variable and localized, quantifying impacts using global models can be challenging Our approach used a regional chemical-transport model at different scales, with high-resolution ship emissions, to evaluate model results against observations and estimate the regional impact of shipping emissions. In the future, additional work is needed in other regions and at different spatial scales (measurements and modeling) in order to investigate the impacts of shipping over the wider Arctic area.

References

Ahmadov, R., McKeen, S., Trainer, M., Banta, R., Brewer, A., Brown, S., Edwards, P. M.,
20 de Gouw, J. A., Frost, G. J., Gilman, J., Helmig, D., Johnson, B., Karion, A., Koss, A., Langford, A., Lerner, B., Olson, J., Oltmans, S., Peischl, J., Pétron, G., Pichugina, Y., Roberts, J. M., Ryerson, T., Schnell, R., Senff, C., Sweeney, C., Thompson, C., Veres, P. R., Warneke, C., Wild, R., Williams, E. J., Yuan, B., and Zamora, R.: Understanding high wintertime ozone pollution events in an oil- and natural gas-producing region of the western US,
25 Atmos. Chem. Phys., 15, 411–429, doi:10.5194/acp-15-411-2015, 2015.
Aliabadi, A. A., Staebler, R. M., and Sharma, S.: Air quality monitoring in communities of the Canadian Arctic during the high shipping season with a focus on local and marine pollution, Atmos. Chem. Phys., 15, 2651–2673, doi:10.5194/acp-15-2651-2015, 2015.
Boucher, O., Randall, D., Artaxo, P., Bretherton, C., Feingold, G., Forster, P., Kerminen, V.-M.,
30 Kondo, Y., Liao, H., Lohmann, U., Rasch, P., Satheesh, S. K., Sherwood, S., Stevens, B.,

Title Page

Abstract | Introduction

Conclusions | References

Tables | Figures

|◄ | ►|

◄ | ►

Back | Close

Full Screen / Esc

Printer-friendly Version

Interactive Discussion

and Zhang, X. Y.: Clouds and aerosols, in: Climate Change 2013: The Physical Science Basis, Contribution of Working Group I to the Fifth Assessment Report of the Intergovernmental Panel on Climate Change, edited by: Stocker, T. F., Qin, D., Plattner, G.-K., Tignor, M., Allen, S. K., Boschung, J., Nauels, A., Xia, Y., Bex, V., and Midgley, P. M., Cambridge University Press, Cambridge, UK and New York, NY, USA, 2013.

Briggs, G. A.: A plume rise model compared with observations, JAPCA J. Air Waste Ma., 15, 433–438, 1965.

Brioude, J., Arnold, D., Stohl, A., Cassiani, M., Morton, D., Seibert, P., Angevine, W., Evan, S., Dingwell, A., Fast, J. D., Easter, R. C., Pisso, I., Burkhart, J., and Wotawa, G.: The Lagrangian particle dispersion model FLEXPART-WRF version 3.1, Geosci. Model Dev., 6, 1889–1904, doi:10.5194/gmd-6-1889-2013, 2013.

Capaldo, K. P., Corbett, J. J., Kasibhatla, P., Fischbeck, P., and Pandis, S. N.: Effects of ship emissions on sulphur cycling and radiative climate forcing over the ocean, Nature, 400, 743–746, 1999.

Cohan, D. S., Hu, Y., and Russell, A. G.: Dependence of ozone sensitivity analysis on grid resolution, Atmos. Environ., 40, 126–135, doi:10.1016/j.atmosenv.2005.09.031, 2006.

Cooper, D. A.: Exhaust emissions from high-speed passenger ferries, Atmos. Environ., 35, 4189–4200, doi:10.1016/S1352-2310(01)00192-3, 2001.

Corbett, J. J. and Fischbeck, P.: Emissions from ships, Science, 278, 823–824, 1997.

Corbett, J. J. and Köhler, H. W.: Updated emissions from ocean shipping, J. Geophys. Res., 108, 4650, doi:10.1029/2003JD003751, 2003.

Corbett, J. J., Winebrake, J. J., Green, E. H., Kasibhatla, P., Eyring, V., and Lauer, A.: Mortality from ship emissions: a global assessment, Environ. Sci. Technol., 41, 8512–8518, doi:10.1021/es071686z, 2007.

Corbett, J. J., Lack, D. A., Winebrake, J. J., Harder, S., Silberman, J. A., and Gold, M.: Arctic shipping emissions inventories and future scenarios, Atmos. Chem. Phys., 10, 9689–9704, doi:10.5194/acp-10-9689-2010, 2010.

Dalsøren, S. B., Endresen, Ø., Isaksen, I. S. A., Gravir, G., and Sørgård, E.: Environmental impacts of an expected increase in sea transportation, with particular focus on oil and gas scenarios for Norway and northwest Russia, J. Geophys. Res., 112, D02310, doi:10.1029/2005JD006927, 2007.

Dalsøren, S. B., Eide, M. S., Endresen, Ø., Mjelde, A., Gravir, G., and Isaksen, I. S. A.: Update on emissions and environmental impacts from the international fleet of ships: the contribution

18438

from major ship types and ports, Atmos. Chem. Phys., 9, 2171–2194, doi:10.5194/acp-9-2171-2009, 2009.

Dalsøren, S. B., Samset, B. H., Myhre, G., Corbett, J. J., Minjares, R., Lack, D., and Fuglestvedt, J. S.: Environmental impacts of shipping in 2030 with a particular focus on the Arctic region, Atmos. Chem. Phys., 13, 1941–1955, doi:10.5194/acp-13-1941-2013, 2013.

Eckhardt, S., Hermansen, O., Grythe, H., Fiebig, M., Stebel, K., Cassiani, M., Baecklund, A., and Stohl, A.: The influence of cruise ship emissions on air pollution in Svalbard – a harbinger of a more polluted Arctic?, Atmos. Chem. Phys., 13, 8401–8409, doi:10.5194/acp-13-8401-2013, 2013.

Emmons, L. K., Walters, S., Hess, P. G., Lamarque, J.-F., Pfister, G. G., Fillmore, D., Granier, C., Guenther, A., Kinnison, D., Laepple, T., Orlando, J., Tie, X., Tyndall, G., Wiedinmyer, C., Baughcum, S. L., and Kloster, S.: Description and evaluation of the Model for Ozone and Related chemical Tracers, version 4 (MOZART-4), Geosci. Model Dev., 3, 43–67, doi:10.5194/gmd-3-43-2010, 2010.

Endresen, Ø., Sørgård, E., Sundet, J. K., Dalsøren, S. B., Isaksen, I. S. A., Berglen, T. F., and Gravir, G.: Emission from international sea transportation and environmental impact, J. Geophys. Res., 108, 4560, doi:10.1029/2002JD002898, 2003.

EPA: Analysis of commercial marine vessels emissions and fuel consumption data, Tech. Rep. EPA420-R-00-002, United States Environmental Protection Agency, available at: http://www.epa.gov/oms/models/nonrdmdl/c-marine/r00002.pdf (last access: 29 June 2015), 2000.

Eyring, V., Stevenson, D. S., Lauer, A., Dentener, F. J., Butler, T., Collins, W. J., Ellingsen, K., Gauss, M., Hauglustaine, D. A., Isaksen, I. S. A., Lawrence, M. G., Richter, A., Rodriguez, J. M., Sanderson, M., Strahan, S. E., Sudo, K., Szopa, S., van Noije, T. P. C., and Wild, O.: Multi-model simulations of the impact of international shipping on Atmospheric Chemistry and Climate in 2000 and 2030, Atmos. Chem. Phys., 7, 757–780, doi:10.5194/acp-7-757-2007, 2007.

Eyring, V., Isaksen, I. S. A., Berntsen, T., Collins, W. J., Corbett, J. J., Endresen, O., Grainger, R. G., Moldanova, J., Schlager, H., and Stevenson, D. S.: Transport impacts on atmosphere and climate: shipping, Atmos. Environ., 44, 4735–4771, doi:10.1016/j.atmosenv.2009.04.059, 2010.

Fast, J. D., Gustafson Jr., W. W. I., Easter, R., Zaveri, R. A., Barnard, J. C., Chapman, E. G., Grell, G., and Peckham, S.: Evolution of ozone, particulates, and aerosol direct radiative forc-

ing in the vicinity of Houston using a fully coupled meteorology–chemistry–aerosol model, J. Geophys. Res., 111, D21305, doi:10.1029/2005JD006721, 2006.

Fuglestvedt, J., Berntsen, T., Eyring, V., Isaksen, I., Lee, D., and Sausen, R.: Shipping emissions: from cooling to warming of climate-and reducing impacts on health, Environ. Sci. Technol., 43, 9057–9062, doi:10.1021/es901944r, 2009.

Fuglestvedt, J. S., Dalsøren, S. B., Samset, B. H., Berntsen, T., Myhre, G., Hodnebrog, Ø., Eide, M. S., and Bergh, T. F.: Climate penalty for shifting shipping to the Arctic, Environ. Sci. Technol., 48, 13273–13279, doi:10.1021/es502379d, 2014.

Granier, C., Niemeier, U., Jungclaus, J. H., Emmons, L., Hess, P., Lamarque, J.-F., Walters, S., and Brasseur, G. P.: Ozone pollution from future ship traffic in the Arctic northern passages, Geophys. Res. Lett., 33, L13807, doi:10.1029/2006GL026180, 2006.

Grell, G. A., Peckham, S. E., Schmitz, R., McKeen, S. A., Frost, G., Skamarock, W. C., and Eder, B.: Fully coupled "online" chemistry within the WRF model, Atmos. Environ., 39, 6957–6975, 2005.

Guenther, A., Karl, T., Harley, P., Wiedinmyer, C., Palmer, P. I., and Geron, C.: Estimates of global terrestrial isoprene emissions using MEGAN (Model of Emissions of Gases and Aerosols from Nature), Atmos. Chem. Phys., 6, 3181–3210, doi:10.5194/acp-6-3181-2006, 2006.

Huszar, P., Cariolle, D., Paoli, R., Halenka, T., Belda, M., Schlager, H., Miksovsky, J., and Pisoft, P.: Modeling the regional impact of ship emissions on NO_x and ozone levels over the Eastern Atlantic and Western Europe using ship plume parameterization, Atmos. Chem. Phys., 10, 6645–6660, doi:10.5194/acp-10-6645-2010, 2010.

IMO: Revised MARPOL Annex VI, Resolution MEP C. 176, available at: http://www.imo.org/blast/blastDataHelper.asp?data_id=23760 (last access: 29 June 2015), 2008.

IMO: Report of the Marine Environment Protection Committee on the Sixty-First Session, Mepc 61/24, IMO (International Maritime Organization), available at: http://docs.imo.org (last access: 29 June 2015), 2010.

Jalkanen, J.-P., Johansson, L., Kukkonen, J., Brink, A., Kalli, J., and Stipa, T.: Extension of an assessment model of ship traffic exhaust emissions for particulate matter and carbon monoxide, Atmos. Chem. Phys., 12, 2641–2659, doi:10.5194/acp-12-2641-2012, 2012.

Jonson, J. E., Jalkanen, J. P., Johansson, L., Gauss, M., and Denier van der Gon, H. A. C.: Model calculations of the effects of present and future emissions of air pollutants from

Title Page

Abstract | Introduction

Conclusions | References

Tables | Figures

|◀ | ▶|

◀ | ▶

Back | Close

Full Screen / Esc

Printer-friendly Version

Interactive Discussion

shipping in the Baltic Sea and the North Sea, Atmos. Chem. Phys., 15, 783–798, doi:10.5194/acp-15-783-2015, 2015.

Lana, A., Bell, T., Simó, R., Vallina, S., Ballabrera-Poy, J., Kettle, A., Dachs, J., Bopp, L., Saltzman, E., Stefels, J., Johnson, J., and Liss, P.: An updated climatology of surface dimethylsulfide concentrations and emission fluxes in the global ocean, Global Biogeochem. Cy., 25, GB1004, doi:10.1029/2010GB003850, 2011.

Lund, M. T., Eyring, V., Fuglestvedt, J. S., Hendricks, J., Lauer, A., Lee, D., and Righi, M.: Global-mean temperature change from shipping toward 2050: improved representation of the indirect aerosol effect in simple climate models, Environ. Sci. Technol., 46, 8868–8877, doi:10.1021/es301166e, 2012.

Lyyranen, J., Jokiniemi, J., Kauppinen, E. I., and Joutsensaari, J.: Aerosol characterisation in medium-speed diesel engines operating with heavy fuel oils, J. Aerosol Sci., 30, 771–784, 1999.

Molders, N., Porter, S., Cahill, C., and Grell, G.: Influence of ship emissions on air quality and input of contaminants in southern Alaska National Parks and wilderness areas during the 2006 tourist season, Atmos. Environ., 44, 1400–1413, doi:10.1016/j.atmosenv.2010.02.003, 2010.

Murrells, T. P., Passant, N. R., Thistlethwaite, G., Wagner, A., Li, Y., Bush, T., Norris, J., Coleman, P. J., Walker, C., Stewart, R. A., Tsagatakis, I., Conolly, C., Brophy, N. C. J., and Okamura, S.: UK Emissions of Air Pollutants 1970 to 2007, AEA, available at: http://naei.defra.gov.uk/reports/reports?report_id=630 (last access: 29 June 2015), 2010.

Nightingale, P., Malin, G., Law, C., Watson, A., Liss, P., Liddicoat, M., Boutin, J., and Upstill-Goddard, R.: In situ evaluation of air–sea gas exchange parameterizations using novel conservative and volatile tracers, Global Biogeochem. Cy., 14, 373–387, 2000.

Ødemark, K., Dalsøren, S. B., Samset, B. H., Berntsen, T. K., Fuglestvedt, J. S., and Myhre, G.: Short-lived climate forcers from current shipping and petroleum activities in the Arctic, Atmos. Chem. Phys., 12, 1979–1993, doi:10.5194/acp-12-1979-2012, 2012.

Peters, G. P., Nilssen, T. B., Lindholt, L., Eide, M. S., Glomsrød, S., Eide, L. I., and Fuglestvedt, J. S.: Future emissions from shipping and petroleum activities in the Arctic, Atmos. Chem. Phys., 11, 5305–5320, doi:10.5194/acp-11-5305-2011, 2011.

Petzold, A., Hasselbach, J., Lauer, P., Baumann, R., Franke, K., Gurk, C., Schlager, H., and Weingartner, E.: Experimental studies on particle emissions from cruising ship, their char-

Title Page

Abstract | Introduction

Conclusions | References

Tables | Figures

|◄ | ►|

◄ | ►

Back | Close

Full Screen / Esc

Printer-friendly Version

Interactive Discussion

acteristic properties, transformation and atmospheric lifetime in the marine boundary layer, Atmos. Chem. Phys., 8, 2387–2403, doi:10.5194/acp-8-2387-2008, 2008.

Prank, M., Sofiev, M., Denier van der Gon, H. A. C., Kaasik, M., Ruuskanen, T. M., and Kukkonen, J.: A refinement of the emission data for Kola Peninsula based on inverse dispersion modelling, Atmos. Chem. Phys., 10, 10849–10865, doi:10.5194/acp-10-10849-2010, 2010.

RINA, Royal Institute of Naval Architects: Significant Ships of 2009, Pensord Press, Blackwood, UK, 2010.

Roiger, A., Thomas, J.-L., Schlager, H., Law, K. S., Kim, J., Schäfler, A., Weinzierl, B., Dahlkötter, F., Krisch, I., Marelle, L., Minikin, A., Raut, J.-C., Reiter, A., Rose, M., Scheibe, M., Stock, P., Baumann, R., Bouarar, I., Clerbaux, C., George, M., Onishi, T., and Flemming, J.: Quantifying emerging local anthropogenic emissions in the Arctic region: the ACCESS aircraft campaign experiment, B. Am. Meteorol. Soc., 96, 441–460, doi:10.1175/BAMS-D-13-00169.1, 2015.

Saide, P. E., Spak, S. N., Carmichael, G. R., Mena-Carrasco, M. A., Yang, Q., Howell, S., Leon, D. C., Snider, J. R., Bandy, A. R., Collett, J. L., Benedict, K. B., de Szoeke, S. P., Hawkins, L. N., Allen, G., Crawford, I., Crosier, J., and Springston, S. R.: Evaluating WRF-Chem aerosol indirect effects in Southeast Pacific marine stratocumulus during VOCALS-REx, Atmos. Chem. Phys., 12, 3045–3064, doi:10.5194/acp-12-3045-2012, 2012.

Saltzman, E. S., King, D. B., Holmen, K., and Leck, C.: Experimental-determination of the diffusion-coefficient of dimethylsulfide in water, J. Geophys. Res.-Oceans, 98, 16481–16486, 1993.

Skamarock, W. C., Klemp, J. B., Dudhia, J., Gill, D. O., Barker, D. M., Duda, M. G., Huang, X. Y., Wang, W., and Powers, J. G.: A Description of the Advanced Research WRF Version 3, Tech. Note, NCAR/TN 475+STR, Natl. Cent. for Atmos. Res., Boulder, Colo., USA, 125 pp., 2008.

Smith, L. and Stephenson, S.: New trans-arctic shipping routes navigable by midcentury, P. Natl. Acad. Sci. USA, 110, E1191–E1195, doi:10.1073/pnas.1214212110, 2013.

Stohl, A., Forster, C., Frank, A., Seibert, P., and Wotawa, G.: Technical note: The Lagrangian particle dispersion model FLEXPART version 6.2, Atmos. Chem. Phys., 5, 2461–2474, doi:10.5194/acp-5-2461-2005, 2005.

Stroeve, J., Serreze, M. C., Holland, M. M., Kay, J. E., Malanik, J., and Barrett, A. P.: The Arctic's rapidly shrinking sea ice cover: a research synthesis, Climatic Change, 110, 1005–1027, doi:10.1007/s10584-011-0101-1, 2011.

Title Page

Abstract | Introduction

Conclusions | References

Tables | Figures

◀ | ▶

◀ | ▶

Back | Close

Full Screen / Esc

Printer-friendly Version

Interactive Discussion

Vinken, G. C. M., Boersma, K. F., Jacob, D. J., and Meijer, E. W.: Accounting for non-linear chemistry of ship plumes in the GEOS-Chem global chemistry transport model, Atmos. Chem. Phys., 11, 11707–11722, doi:10.5194/acp-11-11707-2011, 2011.

Virkkula, A., Hillamo, R. E., Kerminen, V. M., and Stohl, A.: The influence of Kola Peninsula, continental European and marine sources on the number concentrations and scattering co-efficients of the atmospheric aerosol in Finnish Lapland, Boreal Environ. Res., 2, 317–336, 1997.

Wesely, M. L.: Parameterization of surface resistances to gaseous dry deposition in regional-scale numerical models, Atmos. Environ., 23, 1293–1304, 1989.

Winebrake, J., Corbett, J., Green, E., Lauer, A., and Eyring, V.: Mitigating the health impacts of pollution from oceangoing shipping: an assessment of low-sulfur fuel mandates, Environ. Sci. Technol., 43, 4776–4782, doi:10.1021/es803224q, 2009.

Winther, M., Christensen, J. H., Plejdrup, M. S., Ravn, E. S., Eriksson, Ó. F., and Kristensen, H. O.: Emission inventories for ships in the Arctic based on AIS data, Atmos. Environ., 91, 1–14, 2014.

Yang, Q., W. I. Gustafson Jr., Fast, J. D., Wang, H., Easter, R. C., Morrison, H., Lee, Y.-N., Chapman, E. G., Spak, S. N., and Mena-Carrasco, M. A.: Assessing regional scale predictions of aerosols, marine stratocumulus, and their interactions during VOCALS-REx using WRF-Chem, Atmos. Chem. Phys., 11, 11951–11975, doi:10.5194/acp-11-11951-2011, 2011.

Zaveri, R. and Peters, L. K.: A new lumped structure photochemical mechanism for large-scale applications, J. Geophys. Res., 104, 30387–30415, 1999.

Zaveri, R. A., Easter, R. C., Fast, J. D., and Peters, L. K.: Model for Simulating Aerosol Interactions and Chemistry (MOSAIC), J. Geophys. Res., 113, D13204, doi:10.1029/2007JD008792, 2008.

Table 1. Description of the ships sampled during the ACCESS flights on 11 and 12 July 2012.

Ship name	Vessel type	Gross tonnage (tons)	Fuel type
Wilson Leer	Cargo ship	2446	Marine gas oil
Costa Deliziosa	Passenger ship	92 720	Heavy fuel oil
Wilson Nanjing	Cargo ship	6118	Heavy fuel oil
Alaed[*]	Cargo ship	7579	Heavy fuel oil

[*] Ship present in STEAM2, not targeted during the campaign.

Table 2. Parameterizations and options used for the simulations.

Atmospheric process	WRF-Chem option
Planetary Boundary Layer	MYNN (Nakanishi and Niino, 2006)
Surface layer	MM5 Monin–Obukhov scheme, Carlson–Boland viscous sublayer (Carlson and Boland, 1978)
Land surface	Unified Noah land-surface model (Chen and Dudhia, 2001)
Microphysics	Morrison (Morrison, Thompson and Tatarskii, 2009)
Shortwave radiation	Goddard (Chou and Suarez, 1999)
Longwave radiation	RRTM (Mlawer et al., 1997)
Cumulus parameterization	Grell-3 (Grell and Devenyi, 2002)
Photolysis	Fast-J (Wild et al., 2000)
Gas phase chemistry	CBM-Z (Zaveri and Peters, 1999)
Aerosol model	MOSAIC 8 bins (Zaveri et al., 2008)

Table 3. Description of WRF and WRF-Chem simulations.

Name	Description	Period	Remarks
MET	WRF meteorological simulation, 15 km × 15 km resolution (d01)	4–25 July 2012	Nudged to FNL[*]
CTRL	WRF-Chem simulation, HTAPv2 anthropogenic emissions, STEAM2 ship emissions, online MEGAN biogenic emissions, online DMS and sea salt emissions, 15 km × 15 km horizontal resolution (d01)	4–25 July 2012	Nudged to FNL in the free troposphere only
NOSHIPS	CTRL without STEAM2 emissions, 15 km × 15 km horizontal resolution (d01)	4–25 July 2012	Nudged to FNL in the free troposphere only
CTRL3	CTRL setup and emissions, 3 km × 3 km horizontal resolution (d02)	10–12 July 2012	Boundary conditions from CTRL No nudging No cumulus parameterization
NOSHIPS3	NOSHIPS setup and emissions, 3 km × 3 km horizontal resolution (d02)	10–12 July 2012	Boundary conditions from NOSHIPS No nudging No cumulus parameterization

[*] "Final analysis" from the National Centers for Environmental Prediction.

Table 4. NO_x and SO_2 emissions estimated from FLEXPART-WRF and ACCESS measurements, compared with STEAM2 emissions. Values in parentheses indicate the relative difference between STEAM2 and calculated values. SO_2 emissions were not calculated for the *Wilson Leer* and *Alaed* since the measured SO_2 concentrations in the plumes were too low above background.

Ship name	NO_x calculated from measurements ($kg\,day^{-1}$)	NO_x from STEAM2 ($kg\,day^{-1}$)	SO_2 calculated from measurements ($kg\,day^{-1}$)	SO_x from STEAM2 ($kg\,day^{-1}$)
Costa Deliziosa	2728	6767/5243[a] (+148/+92 %[a])	2399	3285/2684[a] (+37/+12 %[a])
Wilson Leer	167/82[b]	287 (+72/+250 %[b])	NA	88 (NA)
Wilson Nanjing	561	602 (+7 %)	504	219 (−57 %)
Alaed	1362	1809 (+33 %)	NA	1130 (NA)

[a] The second value corresponds to STEAM2 calculations using complete technical data from the *Costa Deliziosa* sister ship *Costa Luminosa*.
[b] Value with outliers removed.

Table 5. July emission totals in northern Norway (60.6–73° N, 0 to 31° W) of NO_x, SO_2, BC, OC and $SO_4^=$ in different ship emission inventories.

Inventory	Year	NO_x (kt)	SO_2 (kt)	BC (t)	OC (t)	$SO_4^=$ (t)
STEAM2	2012	7.1	2.4	48.1	123.4	197.3
Winther et al. (2014)	2012	9.3	3.4	47.7	82.9	–
Dalsøren et al. (2009)	2004	3.1	1.9	7.3	24.5	–
Corbett et al. (2010)	2004	2.4	1.6	10.6	32.5	–
Dalsøren et al. (2007)	2000	5.5	1.1	24.	479.3	–

Full Screen / Esc

Printer-friendly Version

Interactive Discussion
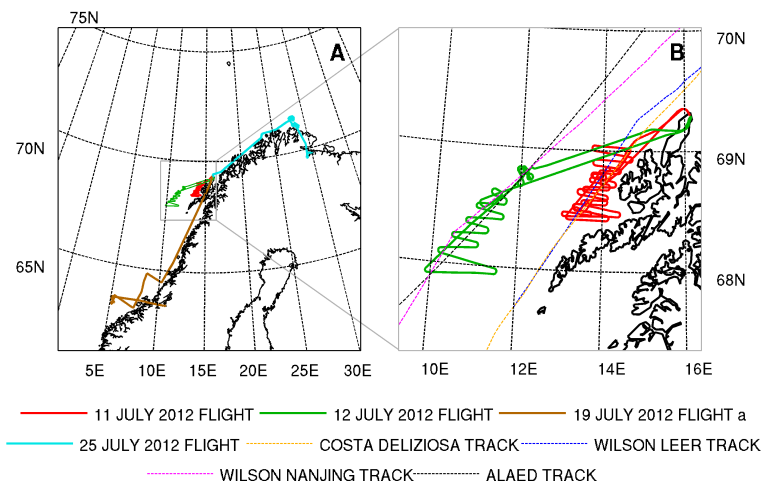
Figure 1. WRF and WRF-Chem domain **(a)** outer domains used for the MET, CTRL, and NO-SHIP runs. ACCESS flight tracks during 11, 12, 19a (a – denotes that this was the first flight that occurred on this day, flight 19b – the second flight was dedicated to hydrocarbon extraction facilities) and 25 July 2012 flights are shown in color. **(b)** Inner domain used for the CTRL3 and NOSHIPS3 simulations, with the tracks of the 4 ships sampled during the 11 and 12 July 2012 flights (routes extracted from the STEAM2 inventory).
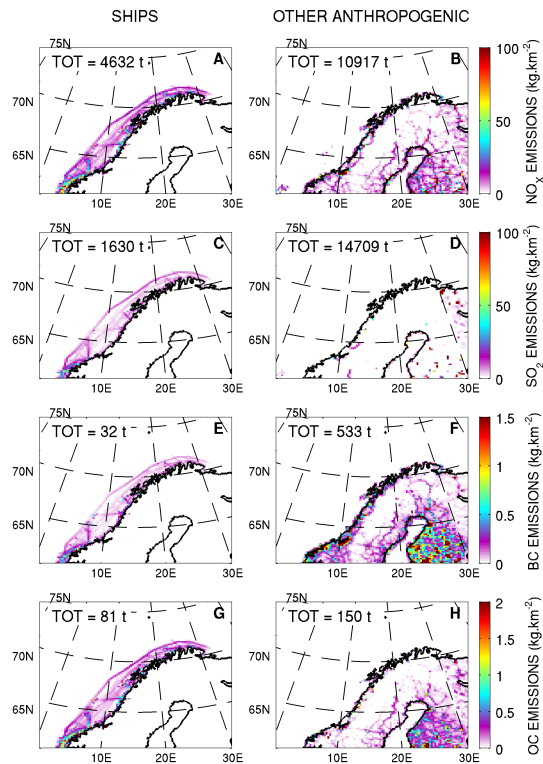
Figure 2. (a, c, e, g) STEAM2 ship emissions and **(b, d, f, h)** HTAPv2 anthropogenic emissions (without ships) of **(a, b)** NO_x, **(c, d)** SO_2, **(e, f)** BC, and **(g, h)** OC in $kg\,km^{-2}$ over the CTRL and NOSHIPS WRF-Chem domain, during the simulation period (00:00 UTC 04 July 2012 to 00:00 UTC 26 July 2012). The emissions totals for the simulation period are noted in each panel.

Title Page

Abstract | Introduction

Conclusions | References

Tables | Figures

|◄ | ►|

◄ | ►

Back | Close

Full Screen / Esc

Printer-friendly Version

Interactive Discussion
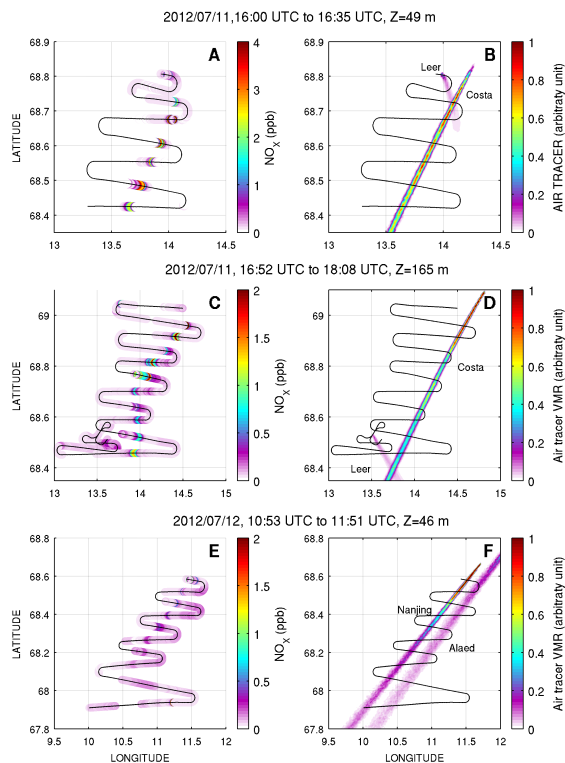
Figure 3. Left panels: ACCESS airborne NO_x measurements between **(a)** 16:00 and 16:35 UTC, 11 July 2012 (flight leg at $Z \sim 49$ m), **(c)** 16:52 and 18:08 UTC, 11 July 2012 ($Z \sim 165$ m), **(e)** 10:53 and 11:51 UTC, 12 July 2012 ($Z \sim 46$ m). Right panels: corresponding FLEXPART-WRF plumes (relative air tracer mixing ratios) **(b, d)** *Wilson Leer* and *Costa Deliziosa* plumes **(f)** *Wilson Nanjing* and *Alaed* plumes. FLEXPART-WRF plumes are shown for the closest model time step and vertical level.
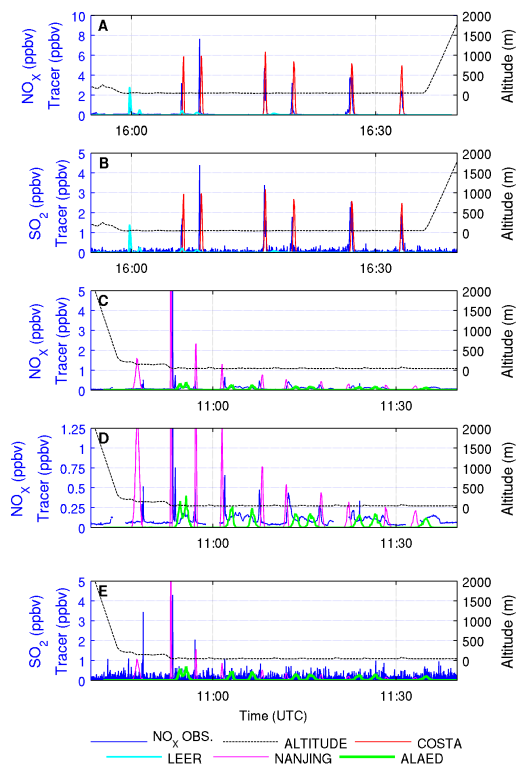
Figure 4. (a, c, d) NO_x and **(b, e)** SO_2 aircraft measurements (dark blue) compared to FLEXPART-WRF air tracer mixing ratios interpolated along flight tracks, for the plumes of the **(a, b)** *Costa Deliziosa* and *Wilson Leer* on 11 July 2012 (first constant altitude level ($Z \sim 49$ m), also shown on Fig. 3a) **(c, d, e)** *Wilson Nanjing* and *Alaed* on 12 July 2012. Panel **(d)** shows the same results as Panel **(c)**, zoomed in. Since model results depend linearly on the emission flux chosen a priori for each ship, model results have been scaled so that peak heights are comparable to the measurements.
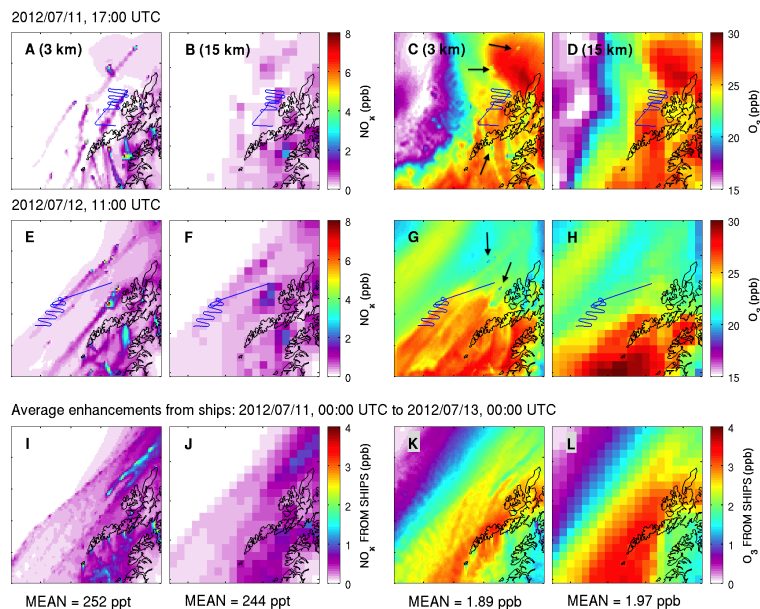
Figure 5. Snapshots of model predicted surface NO$_x$ and O$_3$ from the CTRL3 (3 km) simulation **(a, c, e, g)** and the CTRL (15 km) simulation **(b, d, f, h)** during the flights on 11 and 12 July 2012. Model results for the CTRL3 simulation are shown over the full model domain. CTRL run results are shown over the same region for comparison. The aircraft flight tracks are indicated in blue. On Panels **(c)** and **(g)**, black arrows indicate several areas of O$_3$ titration due to high NO from ships. **(i, j)** NO$_x$ and **(k, l)** O$_3$ 2-day average surface enhancements (00:00 UTC 11 July 2012 to 00:00 UTC 13 July 2012) due to shipping emissions, **(i, k)** CTRL3 simulation, **(j, l)** CTRL simulation. The 2-day average enhancements of NO$_x$ and O$_3$ over the whole area are given below each respective panel.
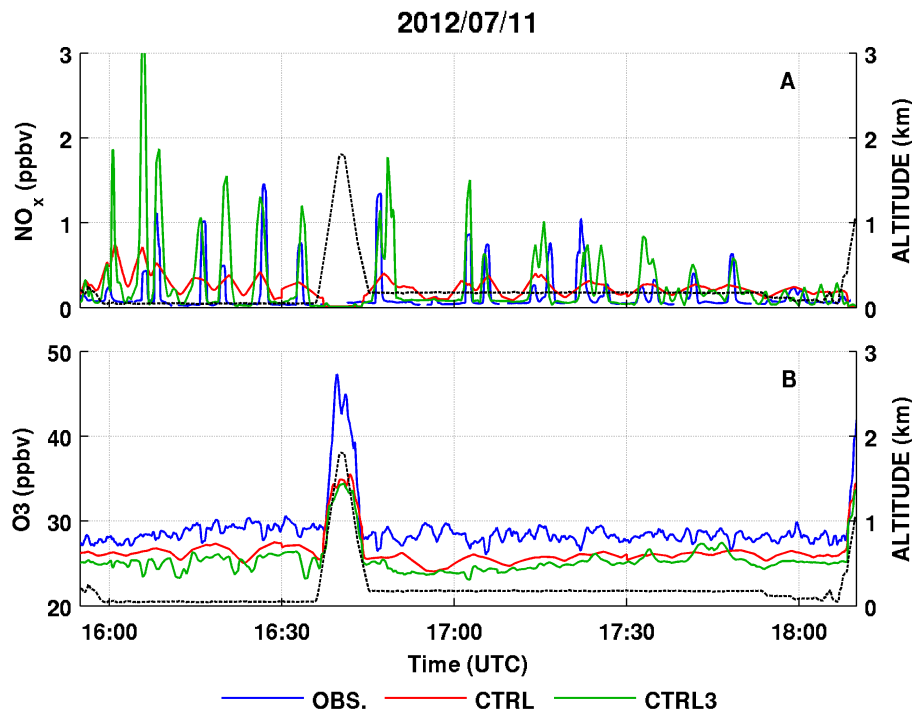
Figure 6. Time series of measured O_3 and NO_x on 11 July 2012 compared to model results extracted along the flight track for the CTRL and CTRL3 runs. Observations are in blue, the CTRL run is in red, and the CTRL3 run is in green. A 56 s averaging window is applied to the measured data for model comparison (approximately the time for the aircraft to travel 2 × 3 km). Flight altitude is given as dashed black line. After the first run at 49 m, a vertical profile was performed (16:35 to 16:45 UTC) providing information about the vertical structure of the boundary layer.

Title Page

Abstract | Introduction

Conclusions | References

Tables | Figures

|◀ | ▶|

◀ | ▶

Back | Close

Full Screen / Esc

Printer-friendly Version

Interactive Discussion
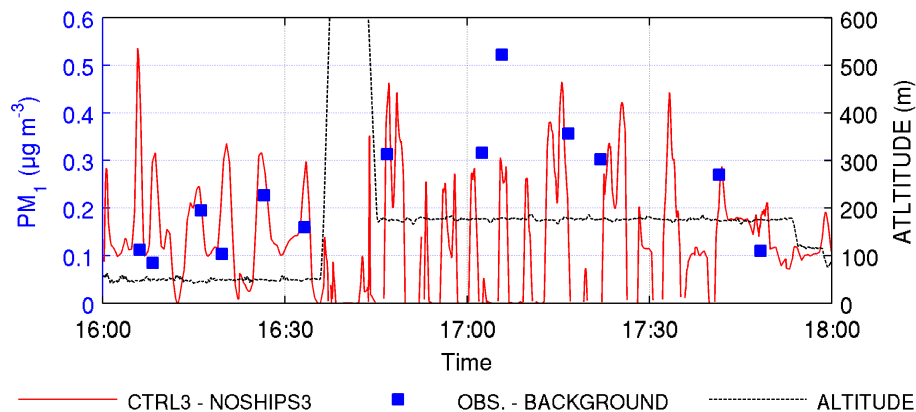
Figure 7. Observed background-corrected PM_1 enhancements in the plume of the *Costa Deliziosa* on 11 July 2012 (blue squares), compared to modeled PM_1 enhancements in ship plumes (in red), extracted along the flight track (CTRL3 – NOSHIPS3 PM_1). A 56 s averaging window is applied to the measured data to simulate dilution in the model grid. Flight altitude is given as dashed black line.

Figure 8. Average vertical profiles of **(a)** NO_x, **(b)** SO_2, **(c)** O_3 and **(d)** $PM_{2.5}$ observed during the 4 ACCESS ship flights (in blue, with error bars showing standard deviations), and interpolated along the ACCESS flight tracks in the CTRL simulation (red line) and in the NOSHIPS simulation (black line). For $PM_{2.5}$ only simulation results are shown.
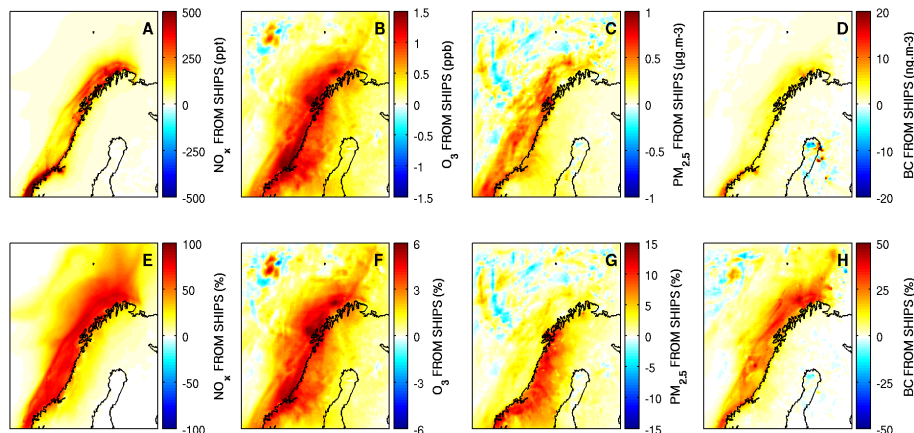
Figure 9. 15 day average (00:00 UTC 11 July 2012 to 00:00 UTC 26 July 2012) of (top) absolute and (bottom) relative surface enhancements (CTRL – NOSHIPS) in **(a, e)** NO_x, **(b, f)** O_3, **(c, g)** $PM_{2.5}$ and **(d, h)** BC due to Norwegian ship emissions from STEAM2.